Received: 4 April 2023 | Revised: 6 July 2023 | Accepted: 24 July 2023

DOI: 10.1111/cbdd.14328

RESEARCH ARTICLE

WILEY

Design and synthesis of novel 1,2,3,4-tetrazines as new anti-leukemia cancer agents

Oznur Eyilcim[1] | **Fulya Gunay**[2] | **Omer Tahir Gunkara**[1] | **Yuk Yin Ng**[2] | **Ozlem Ulucan**[2] | **Ihsan Erden**[3]

[1]Department of Chemistry, Faculty of Science and Arts, Yildiz Technical University, Istanbul, Turkey

[2]Department of Genetics and Bioengineering, Faculty of Engineering and Natural Sciences, Istanbul Bilgi University, Istanbul, Turkey

[3]San Francisco State University, Department of Chemistry & Biochemistry, San Francisco, California, USA

Correspondence
Ihsan Erden, Department of Chemistry & Biochemistry, San Francisco State University 1600 Holloway Avenue, San Francisco, CA 94132, USA.
Email: ierden@sfsu.edu.tr

Funding information
Türkiye Bilimsel ve Teknolojik Araştırma Kurumu

Abstract

A series of novel 1,2,3,4-tetrazines were designed and synthesized. ^{1}H-NMR spectroscopy, ^{13}C NMR spectroscopy, and HRMS were used to determine the structures of this novel compounds. Computational approaches suggested that DHFR is a putative target for the newly synthesized 11 compounds. Extensive molecular dynamics simulations followed by molecular docking simulations were employed to evaluate DHFR as a potential target protein. The anticancer activities of the compounds were evaluated against five different types of leukemia cell lines (Jurkat, Nalm-6, Reh, K562, and Molt-4) and one non-leukemic cell line (Hek293T) by MTT test in vitro and imatinib was used as a control drug. Among these compounds, **3a** exhibited the best activity against all the leukemic cell lines, except Reh cell line. For Nalm-6, K562, Jurkat, and Molt-4 cell lines, IC_{50} values were found to be 15.98, 19.12, 23.15, and 25.80 μM, respectively. Our work focuses on the synthesis of original and novel 1,2,3,4-tetrazine derivatives while contributing to the ongoing effort to discover more potent new antileukemia agents.

KEYWORDS

1,2,3,4-tetrazine renal fibrosis, anticancer activity, azaoxyallyl cations, leukemia cell line, MTT assay

1 | INTRODUCTION

Cancer is a disease of uncontrolled cell proliferation and also major health problem that seriously endangers human life (Siegel et al., 2015). Cancer cases are increasing rapidly around the world and current drugs cannot meet the needs. Heart diseases are considered the primary cause of death, and cancer is expected to outpace heart disease in the next few years (Siegel et al., 2015). Leukemia, as one of the most common human cancer types, has drawn much attention all over the world.

Currently available treatments for cancer are chemotherapy, radiotherapy, and surgery. These treatment methods vary according to the type of cancer, its progression, and the phase of the disease (Jinjun et al., 2017). The most common method used in cancer treatment is chemotherapy. In this method, various drugs are used to treat, control, and alleviate the symptoms of the disease, depending on the type of cancer and its degree of progression. Many of the chemotherapy drugs used affect cell division and proliferation through the control of mitosis and DNA replication and transcription. In addition to having cytotoxic properties, detecting, and destroying cancer cells, and having the least effect on normal cells, chemotherapeutic drugs are the most basic objectives considered during the synthesis of these drugs (Vanneman & Dranoff, 2012). Therefore, the development of new chemotherapy drugs to treat patients is urgently required.

Heterocyclic structures occur widely in many biologically important molecules, and one of them with versatile

nature is tetrazine (Hu et al., 2004). The tetrazine molecule is a compound containing four nitrogen atoms in a six-membered aromatic ring with three isomers as 1,2,3,4-tetrazine, 1,2,3,5-tetrazine, and 1,2,4,5-tetrazine. 1,2,3,4-Tetrazines with thermally unstable structures can be combined with five or six membered rings as well as oxides to increase their stability (Ram et al., 2019) The synthesis of these heterocyclic compounds and their derivatives, due to their a various biological and medicinal properties, are desirable synthetic targets (Wan et al., 2019). One of the isomers, 1,2,4,5-tetrazine, does possess a stable structure and exhibits broader biological activity such as antibacterial, antitumor, anti-inflammatory, anti-malarial, and antiviral (Rao et al., 2013; Nhu et al., 2010; Tabassum et al., 2012; Sauer, 1996). Moreover, there are several studies in the literature concerned with the pharmaceutical use of compounds with 1,2,3,4-tetrazine skeletons (Almerico et al., 2005; Hu et al., 2005; Neunhoeffer, 1985; Zlotin et al., 2015). For example, 1-methyl-3*H*-pyrazolo[1,2-a]benzo[1,2,3,4]tetrazin-3-ones show inhibition of a large number of tumor cell lines at micromole concentrations because of their chemical reactivity (Scheme 1) (Almerico et al., 2005).

There is an increasing need for new antileukemia agents that can be applied in existing chemotherapy methods and will not cause toxic side effects. In this study we synthesized new tetrazine derivatives as possible anticancer agents; furthermore, we evaluated anticancer activities of these synthesized compounds against five important leukemia cell lines. These derivative series were synthesized using 1,3-dipolar cycloaddition reactions of aza-oxyallyl intermediates, generated in situ from α-bromoamides with aryl azides, and the potential anticancer activities of the resulting 1,2,3,4-tetrazines structures were investigated. Jeffrey et al. studied the cycloaddition of different starting materials in the synthesis of nitrogenous heterocyclic compounds with this synthesis procedure they found (An et al., 2016; Cheng et al., 2018; DiPoto et al., 2015; Dipoto & Wu, 2018; Ji, Liu, et al., 2016; Ji, Yao, et al., 2016; Jia et al., 2017; Jiang et al., 2017; Li et al., 2016; Shao et al., 2017).

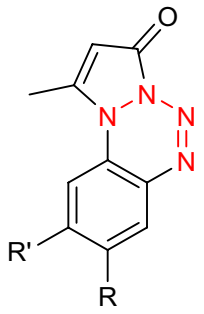

SCHEME 1 1-Methyl-3*H*-pyrazolo[1,2-a]benzo[1,2,3,4]tetrazin-3-ones.

2 | RESULTS AND DISCUSSION

2.1 | Chemistry

Through [3 + 3]-cycloaddition processes, aza-oxyallyl cations are successfully employed as 1,3 dipoles to produce *N*-heterocycles. Scheme 2 shows [3 + 3]-cycloaddition of azides with in situ formed aza-oxyallyl cation to synthesize 1,2,3,4-tetrazines.

The synthesis route designed for the target compounds **3a-j** is outlined in Schemes 3 and 4, based on the methodology developed by Jeffrey et al (Acharya et al., 2013, 2015; Barnes et al., 2014; Jeffrey et al., 2011; Acharya, Eickhoff, et al., 2016; Acharya, Montes, et al., 2016) for generating aza-oxyallyl species.

1,2,3,4-Tetrazine compounds (**3a-j**) were easily prepared following the Lin modification (Scheme 3) (Xu et al., 2018). First, *N*-(benzyloxy)-2-bromo-2-methylpropanamide (compound **1**) was prepared in one step from commercially available 2-bromo-2-methylpropanoyl bromide, and *O*-benzylhydroxylamine hydrochloride. Treatment of 2-bromo-2-methylpropanoyl bromide with *O*-benzylhydroxylamine hydrochloride and Et_3N in CH_2Cl_2 afforded compound **1** (87% yield).

The reactant azide compounds (**2a-j**) were obtained from aromatic or aliphatic amines according to literature procedures (Dai et al., 2015; Lowery et al., 2008; Swetha et al., 2011). Commercially available amines were converted into azide derivatives (**2a-j**) with $NaNO_2$ or NaN_3. All azide derivatives were used directly without any purification. For comparative analysis, the aliphatic chain azide analogues (**2b, 2c, 2d, 2e, 2g**) were also synthesized. Here, it is aimed to determine the effects of different chain lengths on anticancer activity. And also in this study, the effect of different substituents attached to the 1-position of the tetrazine ring on the activity was investigated.

Compound **1** was reacted with various azide compounds (**2a-j**), using sodium carbonate as base, in hexafluoroisopropanol (HFIP) solvent at room temperature to afford the novel 1,2,3,4-tetrazine derivatives (**3a-j**) in good yields. Because fluorinated solvents stabilize the aza-oxyallyl cation, HFIP was used as solvent in these reactions. The crude products were purified by flash column chromatography on silica gel. All the structures of these derivatives were verified by spectral data (^{1}H NMR, ^{13}C NMR, and HRMS).

2.2 | Biological activity

2.2.1 | MTT assay

The anticancer activities of these 11 novel derivatives were tested by the MTT assay in five different leukemia

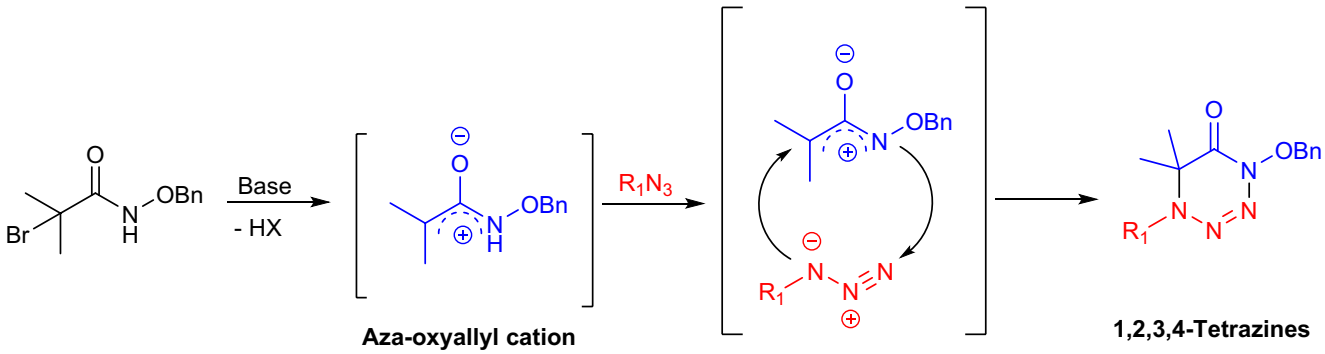

SCHEME 2 Synthesis mechanism of aza-oxyallyl cation.

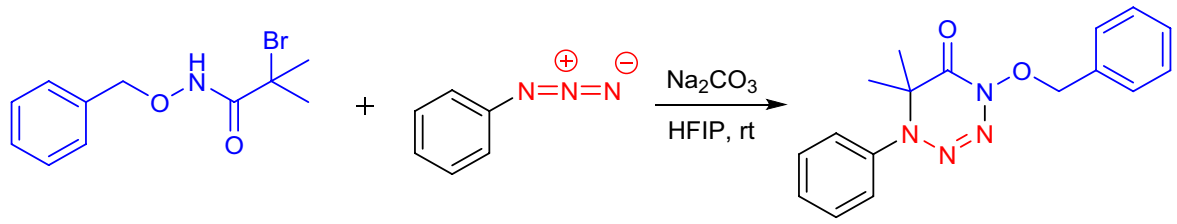

SCHEME 3 Synthesis of novel 1,2,3,4-tetrazine derivatives.

cancer cell lines, including Jurkat, Nalm-6, Reh, K562, and Molt-4, using Imatinib as the positive control. For toxicity control purposes, the activities of all compounds have also been determined on noncancerous, healthy kidney cell lines (HEK293T). The results are shown in Table 1. Compound 3a showed significant high growth inhibition among all the derivatives, except Reh. cell line. Surprisingly, compound 3a exhibited lower IC50 value than Imatinib for K562 cells as 19.12 μM. The designed compound bearing the p-chlorophenyl ring at structure (3a) is much more effective than the compound bearing p-bromophenyl ring (3f). And, novel derivatives compound 3a, 3i, and 3j were effective against Jurkat cells with 23.15, 97.94, 97.98 μM IC50 values, respectively. Compound 3a and Imatinib were equipotent against Nalm-6 and, in general, were more potent than the other derivatives. 3i and 3j derivatives were also found to be more effective than the rest of the derivatives except 3a. Compound 3h, 3i, and 3j gave the best responses in high concentrations against Reh cell line (IC_{50} values were 84.06, 69.93, and 76.54, respectively). Interestingly, these three compounds showed higher efficacy than the positive control cancer drug Imatinib against Reh cells.

As far as structure–activity relationships are concerned, it seems that the presence of a chlorine atom at aromatic ring (compound 3a) were effective especially in K562, Jurkat and Molt-4 cell lines. When the effect of the groups on the aromatic ring is compared, the presence of chlorine atom in the para position increases the activity compared to the presence of bromine or fluorine atoms in the same position. And also it was observed that the compounds were effective against Reh cell line in the presence of fluorine atom in para position on the aromatic ring. It has been determined that derivatives carrying aliphatic side chains have lower potency compared to aromatic ones.

2.3 | Protein target for novel Tetrazine derivatives

Several proteins were identified as targets by the search tool, the Similarity Ensemble Approach (SEA) (Keiser et al., 2007) (see Table S3a). In order to find the most appropriate target protein among all proteins listed by SEA server, we defined several criteria to be met concurrently: (i) the protein must be a human protein or must have a close analog in humans, (ii) the role of the protein in leukemia must be reported by several publications, (iii) the protein must be in the list for compound **3a** since it is the most effective compound among all and (iv) the protein or its homologs must be listed several times by SEA server. DHFR is the only protein that fulfills the criteria listed above. DHFR is a key enzyme in folate metabolism and its role in leukemia has long been known (Banerjee et al., 2002; Dulucq et al., 2008; Matheson et al., 2007; Organista-Nava et al., 2018). Moreover, it is a known drug target, and several approved drugs exist that are inhibitors of DHFR. Among those, **methotrexate**, trimetrexate and pemetrexed bind human DHFR protein and have been used as antineoplastic agents (https://www.drugbank.ca) (Wishart et al., 2006).

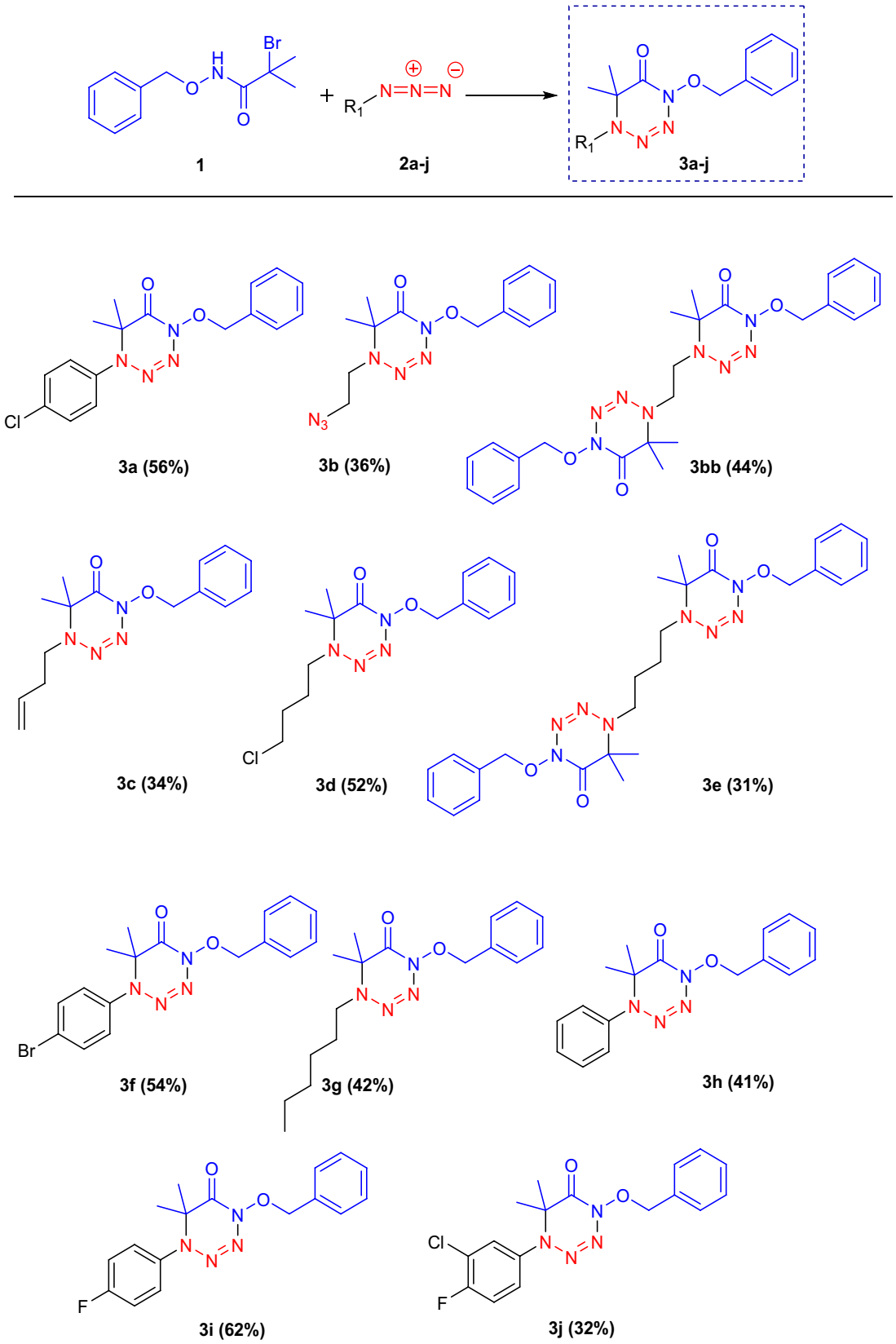

SCHEME 4 Structures of novel 1,2,3,4-tetrazine derivatives.

Figure 1 shows the expression level of the gene DHFR in normal and malignant hematopoietic cells. As seen in the figure, Reh cell line shows the lowest expression level for the gene DHFR, among the leukemia cell lines. We compared the expression level of the gene in each leukemia cell line to the normal hematopoietic cells to determine

TABLE 1 Assay data for 11 new against 1,2,3,4-tetrazines derivatives (**3a-j**), 5 leukemia cell lines (Jurkat, Nalm-6, Reh, K562, Molt-4) and human embryonic kidney cell line (Hek293T).

Comp.	IC_{50} (μM)					
	Jurkat	Nalm-6	Reh	K562	Molt-4	Hek293T
3a	23.15 ± 0.02941	15.98 ± 0.000816	149.8 ± 0.1116	19.12 ± 0.006892	25.8 ± 0.1286	190.0 ± 0.0125
3b	>200	56.99 ± 0.07736	>200	>200	>200	>200
3bb	>200	>200	>200	>200	>200	>200
3c	>200	127.9 ± 0.008876	>200	>200	>200	>200
3d	>200	180.2 ± 0.01558	>200	>200	>200	>200
3e	>200	38.4 ± 0.04895	151.5 ± 0.008998	>200	>200	>200
3f	>200	99.97 ± 0.02723	>200	>200	>200	>200
3g	>200	>200	>200	>200	>200	>200
3h	143.4 ± 0.0406	97.37 ± 0.03778	84.06 ± 0.05566	>200	>200	>200
3i	97.94 ± 0.0276	101.6 ± 0.02473	69.93 ± 0.02595	101.7 ± 0.06008	153.8 ± 0.04584	195.0 ± 0.010
3j	97.98 ± 0.02053	73.55 ± 0.01586	76.54 ± 0.0256	81.48 ± 0.04516	62.61 ± 0.03266	>200
Imatinib*	12.52 ± 0.009645	21.74 ± 0.004601	>200	78.37 ± 0.01842	64.42 ± 0.05326	33.60 ± 0.05468

Note: The data are presented as mean values ±SD from experiments conducted in 6 replicates (**3a-j**).
*Imatinib is positive control drug.

whether the difference is significant. *p*-values and log2 fold change values for those comparisons are tabulated in Table 2. Compared to normal cells, leukemia cell lines overexpress the DHFR gene significantly ($p < 1.0 \times 10^{-3}$). Those results strengthen the prediction that the DHFR is the putative target for the novel tetrazine derivatives.

Table 3 summarizes the results of the 11 compounds docked to the channel of DHFR. We obtained different number of clusters for each compound varying from 3 to 54. Even though binding free energies are higher for compounds **3bb** and **3e**, the high number of clusters together with the small size of the largest cluster renders the results for those two compounds less reliable. The results for compounds **3a**, **3h**, **3f**, and **3i** seem to be converged and therefore are more reliable. Even though we did not obtain a single cluster for those compounds, most of the runs generated very close conformations resulting in a single highly populated cluster. The binding free energies of those compounds for the highest-ranking conformation of the highly populated cluster are −9.6, −9.1, −9.4, and −8.8 kcal/mol for **3a**, **3h**, **3f**, and **3i**, respectively.

Considering the large search space and the randomness in the docking procedure, one should not expect all the independent runs to converge to the same binding conformation. Despite this, we can still use the largest conformational cluster to locate the binding site on DHFR. Figure 2 depicts the binding conformations for all compounds except for compounds **3bb** and **3e**. Even though, we gradually increased the number of maximum energy evaluations to 40 million for those two compounds, we did not observe any improvement in convergence. For the compounds **3a**, **3b**, **3c**, **3d**, **3e**, **3f**, **3g**, **3h**, **3i** and **3j**; even 10 million maximum energy evaluations sufficed to obtain a single highly populated cluster. The analysis of binding conformations showed that the compounds **3h**, **3i** and **3j** bind the same site in the same orientation (Figure 2c), which is expected considering how similar the molecules are. Compounds **3a** and 3f also adopted partially matching orientation (Figure 2b) in the same site that compounds **3h**, **3i** and **3j** bind. Although, the compounds **3b**, **3c**, **3d** and **3g** also bind the same site (Figure 2d) like other compounds, each one adopts a different orientation. Analysis of the docking conformations suggests that the compounds have a tendency to bind the same site. The binding site is close to the middle of the channel and partially overlapping with both binding sites of NAPDH and folic acid (Figure 2a).

For comparison, we performed molecular docking simulations of two approved drugs; **methotrexate**, a folate derivative and trimetrexate, a non-classical folic acid antagonist that bind to human DHFR. We obtained −11.9 and −9.3 kcal/mol binding free energies for **methotrexate** and trimetrexate respectively. Compared to the binding free energies obtained for the

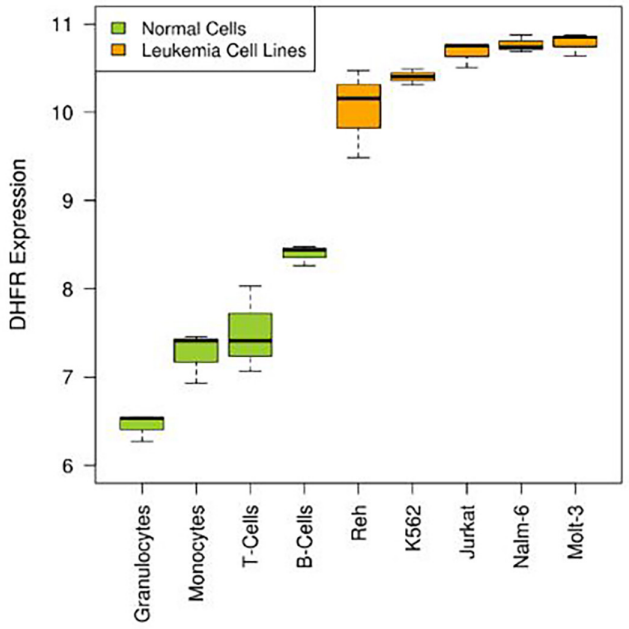

FIGURE 1 Boxplot of log2-transformed and normalized expression values for the DHFR gene generated using the graphics package from R version 3.6.3.

TABLE 2 Comparison of *DHFR* expression level in leukemia cell lines to normal hematopoietic cells.

Cell line	Log fold change	*p*-value
Jurkat	3.3	4.0×10^{-9}
Nalm-6	3.4	3.9×10^{-9}
Reh	2.6	1.0×10^{-3}
K562	3	1.6×10^{-8}
Molt-3	3.2	2.8×10^{-9}

newly synthesized molecules, **methotrexate** has more favorable binding free energy. However, the binding free energy for the trimetrexate is comparable to those for newly synthesized molecules.

Additionally, we conducted molecular dynamics simulations of nine newly synthesized compounds and the reference molecule **methotrexate** in complex with DHFR. All molecules stayed bound to the protein throughout the simulations. We assessed the stability of the docking conformations with RMSD values of the molecules after aligning the protein conformations. Table 4 shows the average RMSD values together with the standard deviations. Considering the average RMSD values, one can see that compounds **3a**, **3h**, and **methotrexate** kept close conformations (rmsd <3.0 Å) to their initial conformations while other compounds adopted slightly different (**3c**, rmsd: 3.5 Å) to quite different (**3f**, rmsd: 7.7 Å) conformations.

To further address the affinities of the molecules to DHFR, we utilized the widely used end-point method Molecular Mechanics/Generalized Born Surface Area (MM/GBSA). The method is commonly used in combination with a method for solute entropy contribution and provides more accurate results compared to scoring functions used in molecular docking. Table 4 provides the components of MMGBSA effective energy and the contribution due to the solute entropy. Computed free energies of binding for the molecules except for compound **3b** vary between −9.4 and −18.3 kcal/mol. The reference molecule **methotrexate** has the most favorable binding free energy followed by the compound **3j** (−16.8 kcal/mol), **3a** (−14.7 kcal/mol), **3f** (13.7 kcal/mol), and **3i** (−12.2 kcal/mol) on average. Even though **methotrexate** has the

TABLE 3 Docking results and assessment of convergence. ΔG corresponds to the binding free energy of the highest-ranking conformation of the largest cluster.

Compound	Number of torsions	Number of clusters	Size of the largest cluster (%)	ΔG (kcal/mol)
3a	4	3	74	−9.6
3b	6	6	62	−8.9
3bb*	9	37	16	−9.8
3c	6	8	42	−8.1
3d	7	13	50	−8.4
3h	4	5	79	−9.1
3g	8	10	69	−7.9
3f	4	4	58	−9.4
3e*	11	54	9	−10.3
3i	4	4	49	−8.8
3j	4	7	33	−9.4
Methotraxate	11	12	67	−11.9
Trimetrexate	8	12	31	−9.3

*No convergence was achieved for those compounds.

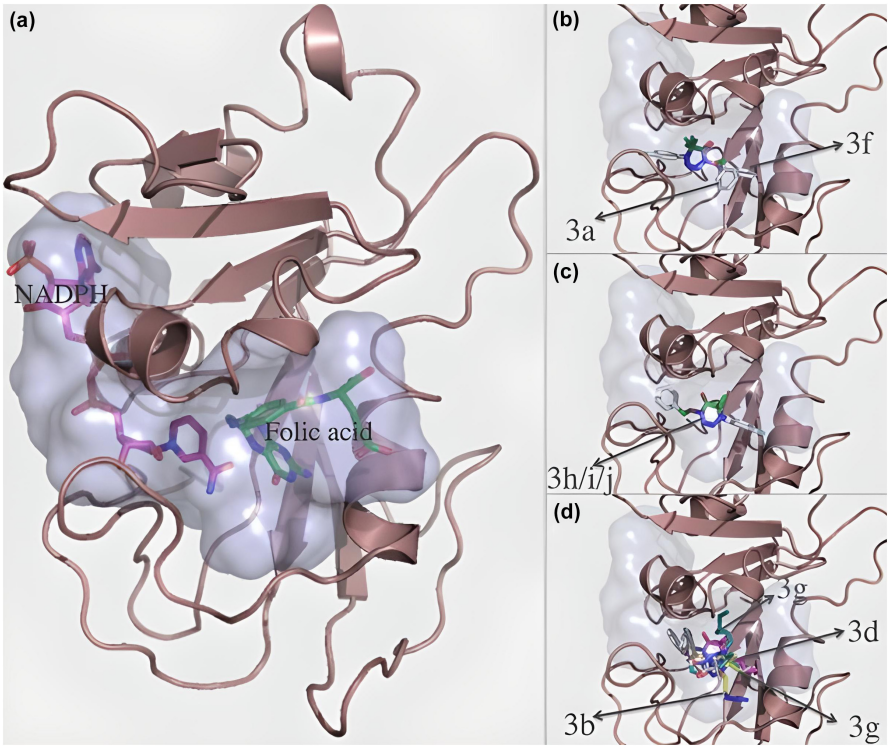

FIGURE 2 The docked conformations to the putative target DHFR. Overall structure of DHFR (depicted in cartoon representation) and the channel detected by the program PROPORES (depicted in light blue surface) are shown. NADPH and folic acid are depicted in stick representation (a). The highest-ranking conformation of the largest cluster for the compounds **3a** and **3f** (b), the compounds **3h**, **3i** and **3j** (c) and **3b**, **3c**, **3d**, and **3g** (d) are shown.

TABLE 4 **Stability assessments and binding free energy calculations.** VdW and EEL stand for Van der Waals and electrostatic interaction energies while EGB and ESURF stand for polar and nonpolar solvation free energies. Total stands for the MMGBSA effective energy and involves solute entropy contribution. The values given in the parenthesis are the standard deviations. 95% Welch–Satterthwaite confidence interval was constructed for free energy of binding as described.

Molecule ID	RMSD (Å)	MMGBSA					Entropy	Binding free energy (kcal/mol)
		VdW	EEL	EGB	ESURF	Total		
3a	2.2 (0.8)	−40.5	−19.0	29.8	−5.0	−34.7 (4.6)	−19.9 (3.6)	−14.7 [−16.6, −12.8]
3b	6.4 (2.2)	−32.5	−5.1	17.2	−4.2	−24.6 (3.2)	−21.5 (5.3)	−3.1 [−5.9, −0.3]
3c	3.5 (0.5)	−34.4	−18.1	29.4	−4.3	−27.4 (3.8)	−16.1 (5.7)	−11.3 [−14.4, −8.2]
3d	5.2 (1.1)	−37.8	−14.4	25.9	−4.8	−31.1 (4.9)	−20.5 (4.5)	−10.6 [−13, −8.2]
3h	2.4 (1.3)	−36.4	−19.7	30.8	−4.5	−29.8 (4.2)	−19.1 (6.5)	−10.7 [−14.2, −7.2]
3g	4.2 (2.2)	−38.3	−6.4	18.2	−4.9	−31.4 (4.2)	−22.1 (5.4)	−9.4 [−12.3, −6.5]
3f	7.7 (1.5)	−40.6	−4.0	15.8	−4.7	−33.5 (4.4)	−19.8 (4.4)	−13.7 [−16, −11.4]
3i	4.2 (1.0)	−36.1	−19.7	29.7	−4.6	−30.7 (4.0)	−18.5 (5.1)	−12.2 [−15, −9.4]
3j	4.2 (2.3)	−43.6	−12.5	23.5	−5.2	−37.8 (3.8)	−21.0 (5.3)	−16.8 [−19.6, −14]
Methotrexate	2.6 (0.5)	−41.2	−357.8	360.0	−6.5	−45.5 (8.0)	−27.2 (12.5)	−18.3 [−26, −10.6]

most favorable binding free energy on average the large error associated to the MMGBSA effective energy and entropic contribution renders the 95% confidence interval considerably large which is expected considering the net charge of the molecule. In such a case where uncertainty is large, it is logical to consider the upper bound for the binding free energy. Accordingly, compound **3j** (<−14 kcal/mol), compound **3a** (<−12.8 kcal/mol) and compound **3f** (<−11.4 kcal/mol) have more favorable binding free energy than the reference molecule **methotrexate** (<−10.6 kcal/mol).

When we consider molecular docking results, stability analysis of bound conformations and binding free energy calculations we see that compound **3a** stands out as the most promising molecule. Therefore, we decided to compare the interactions of the reference molecule **methotrexate** with human DHFR to the interactions of compound **3a** with human DHFR in details. As provided

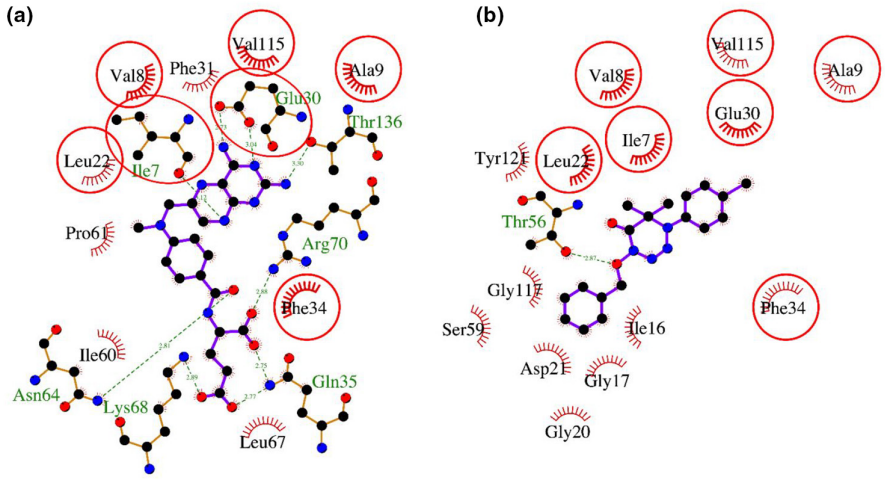

FIGURE 3 Detailed interactions of human DHFR with **methotrexate** (a) and compound **3a** (b). The common contact residues are highlighted with red circles. Hydrogen bonds are shown with dashed lines, while the hydrophobic interactions are indicated by an arc with spokes. The figure was generated using LigPlot+ v.2.2, after energy minimisation of the docked conformation.

in Figure 3, **methotrexate** and compound **3a** interact with 16 and 15 residues on DHFR, respectively. Two molecules have seven interacting residues (Ile 7, Val 8, Ala 9, Leu 22, Glu 34, Phe 34, Val 115) in common. **Methotrexate** and compound **3a** have the same type of interactions with the residues Val 8, Ala 9, Leu 22, Phe 34, and Val 115. In terms of hydrogen bounding, the molecules are quite different. While **methotrexate** forms nine different hydrogen bounds with the protein, compound **3a** forms only one.

3 | CONCLUSION

In this study, we have synthesized novel 1,2,3,4-tetrazines via [3 + 3] cycloaddition reaction between in situ formed aza-oxyallyl cations and azides. Using the Lin (Xu et al., 2018) procedure, we could synthesize several biologically active molecules. MTT assay results showed that 1,2,3,4-tetrazine derivatives have a potential inhibiting effect on the leukemia cell lines; Nalm-6, K562, Jurkat and Molt-4. Especially, compound **3a** showed significantly high growth inhibition on all of the cell lines, except Reh cell line. On K562 cell line, **3a** had lower IC_{50} value than imatinib which has been used as a specific drug for chronic myeloid leukemia. Based on chemical similarity search, DHFR enzyme came out as the putative target for the newly synthesized compounds. Molecular docking simulations, molecular dynamics simulations and binding free energy calculations were performed to evaluate the DHFR as the potential target protein. Compound **3a** came out of computational analysis as the most promising molecule. All together our results suggest that tetrazines have a potential as anticancer agents.

4 | EXPERIMENTAL

4.1 | Chemistry

4.1.1 | General

Unless otherwise stated, nitrogen atmosphere was provided for all reactions carried out in oven-dried glass vessels equipped with magnetic stirring. HFIP and TFE were from Sigma Aldrich and other reagents used in the reactions were obtained from Sigma Aldrich or Merck without any extra processing. Known techniques were used to dry the solvents. Reactions were followed using thin layer chromatography (TLC) on silica gel layers and were detected under UV light. The plates were also visualized by staining with vanillin and $KMnO_4$. Gallenkamp digital thermometer was used to determine all melting points. IR spectra were determined with Perkin Elmer FT-IR spectrometer. Compounds were dissolved in $CDCl_3$ or DMSO-d_6 solvents and the ^1H and ^{13}C NMR spectra of the compounds were obtained using Bruker Avance III-500 MHz NMR spectrometer instrument. Chemical shifts were arranged according to TMS (tetramethylsilane) as an internal standard. Data of ^1H NMR signals are reported as follows: chemical shift, multiplicity as singlet (s), doublet (d), triplet (t), quartet (q), broad (br), multiplet (m), doublet of doublet (dd), doublet of triplet (dt), pentet (p), coupling constants (Hz), number of protons. Mass spectral data were obtained using the Agilent 6890 N/5973 GC/IMSD system and high-resolution mass spectra (HRMS) were determined on an Agilent G6530B TOF/Qtof Mass spectrometer. All final compounds were purified with Teledyne Isco CombiFlash Rf 200 system and RediSep Rf Gold Silica columns.

4.1.2 | General procedure for the synthesis of **1** (Xu et al., 2018)

*N-(Benzyloxy)-2-bromo-2-methylpropanamide (**1**)*

O-Benzylhydroxylamine hydrochloride (0.78 g, 5 mmol) and triethylamine (0.506 g, 5 mmol) dissolved in dichloromethane (0.25 M) and 2-bromo-2-methylpropanoyl bromide (1.15 g, 5 mmol) was added dropwise to the solution at 0°C. The reaction mixture was stirred at this temperature until TLC analysis revealed complete consumption of starting material. The mixture was warmed to room temperature and quenched with water. The organic phase was washed with water (three times), dried over magnesium sulfate, filtered and concentrated. Purification via a column chromatography (SiO_2, 3:1, Hexanes: EtOAc) provided the haloamide in 87% yield as a white solid. $R_f = 0.58$ (3:1, Hexanes: Ethyl Acetate); mp = 88–92°C; FTIR (ATR): $\nu = 3192, 3036, 2956, 2890, 1651, 1497, 1469, 1454, 1112, 1031, 1004\,cm^{-1}$. ^{1}H-NMR (500 MHz, CDCl3): δ 9.02 (brs, 1H), 7.37–7.31 (m, 5H), 4.87 (s, 2H), and 1.86 (s, 6H).

4.1.3 | General procedure for the synthesis of **2a**, **2f**, **2h**, **2i**, and **2j**

The started materials **2a**, **2f**, **2h**, **2i**, and **2j** were prepared using the previously reported method (Dai et al., 2015). Aniline (5 mmol) was dissolved in an ice bath with HCl (3 N, 5 mL). In a separate container, sodium nitrite ($NaNO_2$, 7.5 mmol), dissolved in 12.5 mL water was added dropwise into aniline solution and allowed to stir for 30 minutes. Then sodium azide (NaN_3, 20 mmol), dissolved in 25 mL water, was added dropwise and the reaction was stirred at room temperature for 2–4 h. The resulting mixture was extracted with ethyl acetate, the organic phase washed with water, dried with $MgSO_4$, and the solvent was removed by filtration. The crude product obtained was used for the reaction without purification. The same results were obtained with the spectroscopic data given in the literature (Dai et al., 2015).

*1-Azido-4-chlorobenzene (**2a**)*

It was synthesized according to the general procedure described above. Yield 100%.

*1-Azido-4-bromobenzene (**2f**)*

It was synthesized according to the general procedure described above. Yield 95%.

*Azidobenzene (**2h**)*

It was synthesized according to the general procedure described above. Yield 99%.

*1-Azido-4-fluorobenzene (**2i**)*

It was synthesized according to the general procedure described above. Yield 90%.

*4-Azido-2-chloro-1-fluorobenzene (**2j**)*

It was synthesized according to the general procedure described above. Yield 85%.

4.1.4 | General procedure for the synthesis of **2b** and **2c**

The started materials **2b** and **2c** were prepared using the previously reported method (Swetha et al., 2011). Sodium azide (NaN_3, 0.22 mmol), dissolved in 25 mL water was added to an alkyl halide (0.15 mmol) solution dissolved in 6 mL THF. The reaction mixture was refluxed by heating and the reaction was followed by TLC. After the alkyl halide was completely consumed, the reaction mixture was allowed to cool to room temperature and was extracted using a separatory funnel. The upper layer was separated by extraction with the help of a separatory funnel, washed with water and dried with $MgSO_4$. After filtration, the solvent was evaporated. The crude product was used without purification. The same results were obtained with the spectroscopic data given in the literature (Swetha et al., 2011).

*1,2-Diazidoethane (**2b**)*

It was synthesized according to the general procedure described above. Yield 76%.

*4-Azido-1-butene (**2c**)*

It was synthesized according to the general procedure described above. Yield 86%.

4.1.5 | General procedure for the synthesis of **2d**, **2e**, and **2g**

The starting materials ***2d, 2e, and 2g*** were prepared using the previously reported method (Lowery et al., 2008) Sodium azide (NaN_3, 7.7 mmol) was added to the alkyl halide (7.7 mmol) solution dissolved in 10 mL DMF at room temperature and stirred for 20 h. The reaction was monitored by TLC and after the alkyl halide was completely consumed, the reaction was extracted with ether. The organic phases were combined, washed with water, dried over $MgSO_4$ and the solvent was removed. The residual crude product was used directly without purification.

*1-Azido-4-chlorobutane (**2d**)*

It was synthesized according to the general procedure described above. Yield 94%. ^{1}H NMR (400 MHz, $CDCl_3$) δ = 1.76 (m, 2H), 1.87 (m, 2H), 3.36 (t, J = 6.6 Hz, 2H), 3.53 (t, J = 6.5 Hz, 2H) ppm.

*1,4-Diazidobutane (**2e**)*

It was synthesized according to the general procedure described above. Yield 99%.

*1-Azidohexane (**2g**)*

It was synthesized according to the general procedure described above. Yield 88%.

4.1.6 | General procedure for the synthesis of 1,2,3,4-tetrazines (**3a-j**)

To a Schlenk tube were sequentially added *N*-(benzyloxy)-2-bromo-2-methylpropanamide **1** (0.15 mmol, 0.6 equiv), azides **2a-j** (0.125 mmol, 0.5 equiv), Na_2CO_3 (0.25 mmol, 1.0 equiv) and HFIP (0.5 mL). The Schlenk tube was closed and allowed to stir overnight under nitrogen gas and at room temperature. Once the azides were completely consumed, the reaction mixture was diluted with dichloromethane, filtered through Celite and washed with dichloromethane. The solvent was removed under reduced pressure and the crude product was purified by flash column chromatography on silica gel to give the pure product.

*4-(Benzyloxy)-1-(4-chlorophenyl)-6,6-dimethyl-1,6-dihydro-1,2,3,4-tetrazin-5(4H)-one (**3a**)*

It was synthesized according to the general procedure described above. The product (42.4 mg, 56% yield) as yellowish oil was purified with flash chromatography. $R_f = 0.35$ (EA/H = 1:2). IR (cm^{-1}) $n = 3064$, 3032, 2925, 1688, 1596, 1464, 1354, 1260, 1103. ^{1}H NMR (500 MHz, $CDCl_3$) $\delta = 1.39$ (s, 6H, 2xCH_3), 5.07 (s, 2H, O-CH_2), 6.57 (d, J = 8.2 Hz, 1H, HAr), 6.86 (dd, J = 2.2;8.2 Hz, 1H, HAr), 7.10 (d, J = 2.2 Hz, 1H, HAr), 7.30–7.42 (m, 6H, HAr). ^{13}C NMR (125 MHz, $CDCl_3$) $\delta = 26.1$ (2xCH_3), 50.6 (CH_2), 67.6 (Cq), 116.5 (CAr), 123.5 (CAr), 124.4 (Cq), 127.8 (CAr), 128.3 (2xCAr), 128.4 (2xCAr), 128.7 (CAr), 131.4 (CAr), 137.6 (Cq), 141.5 (Cq), 151.1 (C=O). HRMS (ESI) *m/z* calcd for $[C_{17}H_{17}ClN_4O_2\text{-}N_2 + H]^+$ 317.1057, found 317.1043.

*1-(2-Azidoethyl)-4-(benzyloxy)-6,6-dimethyl-1,6-dihydro-1,2,3,4-tetrazin-5(4H)-one (**3b**)*

It was synthesized according to the general procedure described above. The product (27.3 mg, 36% yield) as yellowish oil was purified with flash chromatography. $R_f = 0.26$ (EA/H = 1:3). IR (cm^{-1}) $n = 3064$, 3033, 2936, 2875, 2097, 1715, 1454, 1367, 1349, 1196, 1034. ^{1}H NMR (500 MHz, $CDCl_3$) $\delta = 1.34$ (s, 6H, 2xCH_3), 3.51–3.53 (m, 2H, CH_2), 3.56–3.59 (m, 2H, CH_2), 5.13 (brds, 2H, O-CH_2), 7.34–7.38 (m, 3H, HAr), 7.47–7.49 (m, 2H, HAr). ^{13}C NMR (125 MHz, $CDCl_3$) $\delta = 20.6$ (2xCH_3), 48.0 (CH_2), 50.0 (CH_2), 59.9 (Cq), 78.7 (O-CH_2), 128.5 (2xCAr), 129.1 (CAr), 129.8 (2xCAr) 133.7 (Cq), 162.5 (C=O). HRMS (ESI) *m/z* calcd for $[C_{13}H_{17}N_7O_2\text{-}N_2 + H]^+$ 276.1460, found 276.1442.

*1,1′-(Ethane-1,2-diyl)bis(4-(benzyloxy)-6,6-dimethyl-1,6-dihydro-1,2,3,4-tetrazin-5(4H)-one) (**3bb**)*

It was synthesized according to the general procedure described above. The product (54.4 mg, 44% yield) as yellowish oil was purified with flash chromatography. $R_f = 0.68$ (EA/H = 1:3). IR (cm^{-1}) $n = 3066$, 3048, 2991, 2956, 2937, 2894, 1713, 1491, 1468, 1389, 1318, 1195, 1058. ^{1}H NMR (500 MHz, $CDCl_3$) $\delta = 1.27$ (s, 12H, 4xCH_3), 3.63 (s, 4H, 2xCH_2), 5.12 (brds, 4H, 2xO-CH_2), 7.35–7.38 (m, 6H, HAr), 7.46–7.49 (m, 4H, HAr). ^{13}C NMR (125 MHz, $CDCl_3$) $\delta = 20.7$ (4xCH_3), 47.6 (2xCH_2), 60.0 (2xCq), 78.5 (2xOCH_2), 128.5 (4xCAr), 129.1 (2xCAr), 129.6 (4xCAr) 133.8 (2xCq), 162.6 (2xC=O). HRMS (ESI) *m/z* calcd for $[C_{24}H_{30}N_8O_4 + H]^+$ 495.2468, found 495.2454.

*4-(Benzyloxy)-1-(but-3-en-1-yl)-6,6-dimethyl-1,6-dihydro-1,2,3,4-tetrazin-5(4H)-one (**3c**)*

It was synthesized according to the general procedure described above. The product (24.5 mg, 34% yield) as yellowish oil was purified with flash chromatography. $R_f = 0.67$ (EA/H = 1:3). IR (cm^{-1}) $n = 3063$, 3032, 2975, 2932, 2876, 1703, 1586, 1464, 1381, 1328, 1213, 1180. ^{1}H NMR (500 MHz, $CDCl_3$) $\delta = 1.32$ (s, 6H, 2xCH_3), 2.45–2.49 (m, 2H, CH_2), 3.41 (t, J = 5.8 Hz, 2H, N-CH_2), 5.06–5.13 (m, 4H, O-CH_2 and =CH_2), 5.74–5.82 (m, 1H, =CH), 7.35–7.39 (m, 3H, HAr), 7.46–7.50 (m, 2H, HAr). ^{13}C NMR (125 MHz, $CDCl_3$) $\delta = 20.5$ (CH_3), 20.6 (CH_3), 34.1 (CH_2), 48.4 (CH_2), 59.8 (Cq), 78.4 (OCH_2), 117.26 (=CH_2), 128.4 (2xCAr), 129.0 (CAr), 129.8 (2xCAr) 133.8 (Cq), 134.6 (=CH), 162.1 (C=O). HRMS (ESI) *m/z* calcd for $[C_{15}H_{20}N_4O_2\text{-}N_2 + H]^+$ 261.1603, found 261.1587.

*4-(Benzyloxy)-1-(4-chlorobutyl)-6,6-dimethyl-1,6-dihydro-1,2,3,4-tetrazin-5(4H)-one (**3d**)*

It was synthesized according to the general procedure described above. The product (42.2 mg, 52% yield) as yellowish oil was purified with flash chromatography. $R_f = 0.54$ (EA/H = 1:3). IR (cm^{-1}) $n = 3089$, 3064, 3032, 2941, 2873, 1713, 1455, 1386, 1315, 1210, 1082. ^{1}H NMR (500 MHz, $CDCl_3$) $\delta = 1.38$ (s, 6H, 2xCH_3), 1.78–1.89 (m, 4H, 2xCH_2), 3.38 (t, J = 7.3 Hz, 2H, N-CH_2), 3.56 (t, J = 7.2 Hz, 2H, Cl-CH_2), 5.14 (s, 2H, O-CH_2), 7.35–7.38 (m, 3H, HAr), 7.47–7.50 (m, 2H, HAr) ppm. ^{13}C NMR (125 MHz, $CDCl_3$) $\delta = 20.4$ (CH_3), 20.5 (CH_3), 27.0 (CH_2), 29.5 (CH_2), 44.5 (CH_2), 48.1 (CH_2), 59.8 (Cq), 78.5 (O-CH_2), 128.5 (2xCAr), 129.1 (CAr), 129.8 (2xCAr), 133.8 (Cq), 162.2 (C=O). HRMS (ESI) *m/z* calcd for $[C_{15}H_{21}ClN_4O_2 + Na)^+$ 347.1251, found 347.1242.

*1,1′-(Butane-1,4-diyl)bis(4-(benzyloxy)-6,6-dimethyl-1,6-dihydro-1,2,3,4-tetrazin-5(4H)-one) (**3e**)*

It was synthesized according to the general procedure described above. The product (40.5 mg, 31% yield) as colorless oil was purified with flash chromatography. $R_f = 0.34$ (EA/H = 1:3). IR (cm^{-1}) $n = 3063$, 3032, 2941, 2874, 1709, 1553, 1480, 1454, 1367, 1257, 1027. ^{1}H NMR (500 MHz, $CDCl_3$) $\delta = 1.32$ (s, 12H, 4xCH_3), 1.62–1.66 (m, 2H, CH_2), 1.80 (pent, J = 7.4 Hz, 2H, CH_2), 3.32 (t, J = 7.0 Hz, 2H, N-CH_2), 3.38 (t, J = 7.0 Hz, 2H, N-CH_2), 5.14 (s, 4H, O-CH_2), 7.35–7.39 (m, 6H, ArH), 7.47–7.49 (m, 4H, ArH). ^{13}C NMR (125 MHz, $CDCl_3$) $\delta = 20.5$ (4xCH_3), 26.0 (CH_2), 26.9

(CH_2), 48.2 (N-CH_2), 51.1 (N-CH_2), 59.8 (2xCq), 78.5 (2xO-CH_2), 128.5 (4xCAr), 129.1 (2xCAr), 129.8 (4xCAr), 133.8 (2xCq), 162.2 (2xC=O). HRMS (ESI-QTOF) *m/z* calcd for $[C_{26}H_{34}N_8O_4\text{-}N_4+Na]^+$ 489.2478, found 489.2472.

*4-(Benzyloxy)-1-(4-bromophenyl)-6,6-dimethyl-1,6-dihydro-1,2,3,4-tetrazin-5(4H)-one (**3f**)*

It was synthesized according to the general procedure described above. The product (52.4 mg, 54% yield) as yellowish oil was purified with flash chromatography. R_f = 0.55 (EA/H = 1:3). IR (cm^{-1}) *n* = 3088, 3063, 3031, 2974, 2926, 2872, 1704, 1588, 1453, 1400, 1385, 1251, 1067. ^{1}H NMR (500 MHz, $CDCl_3$) δ = 1.39 (s, 6H, 2xCH_3), 5.07 (s, 2H, O-CH_2), 6.52 (d, J = 8.2 Hz, 1H, HAr), 6.99 (dd, J = 2.2; 8.2 Hz, 1H, ArH), 7.23 (d, J = 2.2 Hz, 1H, ArH), 7.28–7.38 (m, 6H, ArH). ^{13}C NMR (125 MHz, $CDCl_3$) δ = 26.1 (2xCH_3), 50.6 (CH2), 63.0 (Cq), 111.0 (Cq), 116.9 (CAr), 119.3 (CAr), 126.4 (CAr), 127.8 (CAr), 128.3 (CAr), 128.4 (CAr), 128.7 (2xCAr), 129.7 (CAr), 130.9 (Cq), 141.7 (Cq), 151.1 (C=O). HRMS (ESI) *m/z* calcd for $[C_{17}H_{17}BrN_4O_2\text{-}N_2+H]^+$ 361.0552, found 361.0543.

*4-(Benzyloxy)-1-hexyl-6,6-dimethyl-1,6-dihydro-1,2,3,4-tetrazin-5(4H)-one (**3g**)*

It was synthesized according to the general procedure described above. The product (33.4 mg, 42% yield) as yellowish oil was purified with flash chromatography. R_f = 0.50 (EA/H = 1:3). IR (cm^{-1}) *n* = 3033, 2953, 2929, 2870, 1715, 1497, 1455, 1377, 1316, 1151, 1027. ^{1}H NMR (500 MHz, $CDCl_3$) δ = 0.90 (t, J = 6.9 Hz, 3H, CH_3), 1.29–1.36 (m, 12H, 2xCH_3 and 3xCH_2), 1.70 (pent, J = 8.2 Hz, 2H, CH_2), 3.34 (t, J = 7.6 Hz, 2H, N-CH_2), 5.14 (s, 2H, O-CH_2), 7.35–7.39 (m, 3H, HAr), 7.47–7.50 (m, 2H, HAr). ^{13}C NMR (125 MHz, $CDCl_3$) δ = 14.0 (CH_3), 20.6 (2xCH_3), 22.5 (CH_2), 26.3 (CH_2), 29.8 (CH_2), 31.5 (CH_2), 49.0 (CH_2), 59.8 (Cq), 78.4 (O-CH_2), 128.4 (2xCAr), 129.0 (CAr), 129.8 (2xCAr), 133.9 (Cq), 162.0 (C=O). HRMS (ESI) *m/z* calcd for $[C_{17}H_{26}N_4O_2\text{-}N_2+H]^+$ 291.2073, found 291.2063.

*4-(Benzyloxy)-6,6-dimethyl-1-phenyl-1,6-dihydro-1,2,3,4-tetrazin-5(4H)-one (**3h**)*

It was synthesized according to the general procedure described above. The product (31.8 mg, 41% yield) as colorless oil was purified with flash chromatography. R_f = 0.60 (EA/H = 1:3). IR (cm^{-1}) *n* = 3062, 3031, 2973, 2924, 2872, 1703, 1499, 1454, 1384, 1365, 1213, 1081. ^{1}H NMR (500 MHz, $CDCl_3$) δ = 1.41 (s, 6H, 2xCH_3), 5.08 (s, 2H, CH_2), 6.65 (dd, J 1.5; 7.8 Hz, 1H, ArH), 6.78 (dt, J 1.5; 7.8 Hz, 1H, ArH), 6.89 (dt, 1.56; 7.56 Hz, 1H, ArH), 7.07 (dd, J 1.26; 8.19 Hz, 1H, ArH), 7.31 (m, 3H, ArH), 7.39 (m, 3H, ArH). ^{13}C NMR (125 MHz, $CDCl_3$) δ = 26.2 (CH_3), 26.2 (CH_3), 50.7 (CH_2), 61.2 (Cq), 115.9 (CAr), 116.1 (CAr), 120.0 (CAr), 123.6 (CAr), 127.7 (CAr), 128.2 (2xCAr), 128.36 (2xCAr), 128.4 (CAr), 131.7 (Cq), 137.9 (Cq), 170.5 (C=O). HRMS (ESI) *m/z* calcd for $[C_{17}H_{18}N_4O_2\text{-}N_2+H]^+$ 283.1447, found 283.1437.

*4-(Benzyloxy)-1-(4-fluorophenyl)-6,6-dimethyl-1,6-dihydro-1,2,3,4-tetrazin-5(4H)-one (**3i**)*

It was synthesized according to the general procedure described above. The product (50.9 mg, 62% yield) as yellowish oil was purified with flash chromatography. R_f = 0.44 (EA/H = 1:3). IR (cm^{-1}) *n* = 3065, 3032, 2974, 2928, 2871, 1709, 1506, 1454, 1384, 1326, 1263, 1134. ^{1}H NMR (500 MHz, $CDCl_3$) δ = 1.38 (s, 6H, 2xCH_3), 5.06 (s, 2H, CH_2), 6.58–6.66 (m, 2H, ArH), 6.84 (dd, J 2.6; 9.1 Hz, 1H, ArH), 7.27–7.31 (m, 1H, ArH), 7.33–7.38 (m, 3H, ArH), 7.40–7.43 (m, 2H, ArH). ^{13}C NMR (125 MHz, $CDCl_3$) δ = 25.9 (2xCH_3), 50.6 (CH_2), 59.7 (Cq), 103.9 (CAr), 110.0 (CAr), 116.6 (CAr), 127.9 (CAr), 128.3 (2xCAr), 128.5 (2xCAr), 129.7 (CAr), 137.6 (Cq), 153.3 (Cq), 157.7 (Cq), 171.4 (C=O). HRMS (ESI) *m/z* calcd for $[C_{17}H_{17}FN_4O_2\text{-}N_2+H]^+$ 301.1352, found 301.1350.

*4-(Benzyloxy)-1-(3-chloro-4-fluorophenyl)-6,6-dimethyl-1,6-dihydro-1,2,3,4-tetrazin-5(4H)-one (**3j**)*

It was synthesized according to the general procedure described above. The product (29.0 mg, 32% yield) as yellowish oil was purified with flash chromatography. R_f = 0.42 (EA/H = 1:3). IR (cm^{-1}) *n* = 3065, 3033, 2990, 2942, 2881, 1716, 1592, 1494, 1455, 1384, 1263, 1030. ^{1}H NMR (500 MHz, $CDCl_3$) δ = 1.27 (s, 6H, 2xCH_3), 5.20 (s, 2H, CH_2), 7.18–7.21 (m, 2H, ArH), 7.38–7.40 (m, 4H, ArH), 7.51–7.53 (m, 2H, ArH). ^{13}C NMR (125 MHz, $CDCl_3$) δ = 20.9 (2xCH_3), 60.9 (CH_2), 66.4 (Cq), 116.6 (CAr), 116.8 (CAr), 128.5 (2xCAr), 129.2 (CAr), 129.8 (2xCAr), 130.5 (CAr), 133.6 (Cq), 137.5 (Cq), 158.7 (Cq), 162.1 (Cq), 171.0 (C=O). HRMS (ESI) *m/z* calcd for $[C_{17}H_{16}ClFN_4O_2\text{-}N_2+H]^+$ 335.0963, found 335.0937.

4.2 | MTT assay study

4.2.1 | Cell lines and culture condition

Culturing of K562 and Nalm-6 cell lines in RPMI medium was performed, culturing of Jurkat and Molt4 cell lines in DMEM medium and culturing of Hek293T cell line in Iscove Basal medium. All type of mediums was supplemented with 10% heat inactivated fetal bovine serum, 1% penicillin and streptomycin and all the cells were incubated at 5% CO_2 and 37°C.

4.2.2 | Cell proliferation assay

MTT assay was used to evaluate the growth inhibition effect of the compounds on various cell lines (Cory et al., 1991) Cells were re-suspended in medium, counted in Biorad TC20 Automated Cell Couter device, and seeded as 5×10^5 cells/ml for leukemic cell lines and as 1×10^5 cells/ml for non-leukemic cell line in 96 well plates and incubated over-night.

Stock solutions (33.3–10–5–1 mM and 300 μM) of all the compounds were firstly dissolved in DMSO according to their molecular weight, and then they were diluted with related medium for adjusting the desired concentration before adding to the cells. The DMSO rate of the total solution does not exceed 1.2% because of its toxicity. A proliferation assay with increasing concentrations (1–3–5-10-15-20-30-50-70-100-150-200 μM) were applied to cells as six replicates. And then, the cells were incubated with various concentrations of compounds for 24 h.

After incubation, 100 μL of supernatant was removed from each well and 10 μL of MTT solution (5 mg/mL) was added to each well and incubated at 37°C for 4 h. The 50 μL of supernatant was discarded from each well and 100 μL of DMSO was added to dissolve formazan produced by living cells. Plates were shaken for 45 minutes to dissolve it. Then the optical density of each well was measured by using Thermo VarioSkan Flush Multimode Reader Quantum ST5-1100 at 570 nm wavelength. The IC_{50} values were calculated by using Graphpad Prism. Viability rate (VR), was calculated by the following formula from the spectrophotometric results.

$$\%\,\mathrm{VR} = 100 - \frac{\left(\mathrm{OD}_{(\mathrm{control})} - \mathrm{OD}_{(\mathrm{sample})}\right)}{\mathrm{OD}_{(\mathrm{control})}} \times 100$$

4.2.3 | Statistical analyses for IC_{50}

The IC_{50} values were calculated by using GraphPad Prism. All the data presented as the mean of 6 replicates. Results were analyzed and illustrated with Graph Pad Prism (version 5; GraphPad Software, San Diego, CA, USA). Statistical analysis was performed using dose–response inhibition, log(inhibitor) versus response-variable slope, least squares (ordinary) fit.

4.3 | Docking study

4.3.1 | Computational methods

Prediction of target protein

In order to predict putative targets for the novel tetrazine derivatives, we used Similarity Ensemble Approach (SEA, www.sea.bkslab.org) online search tool provided by Shoichet Laboratory in the Department of Pharmaceutical Chemistry at the University of California (Keiser et al., 2007). SMILES for the compounds were uploaded to the SEA server all together to search for protein targets based on chemical similarity.

DHFR expression analysis

Raw data for normal (granulocytes, monocytes, T-cells and B-cells) and malignant hematopoietic cells were obtained from Gene Expression Omnibus (GEO) using the accession number GSE48558 (see Table S3b). Since we could not find raw data for Molt-4 cell line that were generated using Affymetrix Human Gene 1.0 ST-Array, we included the raw data from Molt-3 cell line, which was also derived from the same patient that the Molt-4 cell line was derived (Greenberg et al., 1988). The raw data were normalized using the Robust Multi-array Average (RMA) method, which is part of the R package oligo (Carvalho & Irizarry, 2010) The Affimetrix Probe IDs were mapped to Ensembl IDs with the help of hugene10sttranscriptcluster.db annotation package in R. The normalized and log2-transformed expression values for the gene Dihydrofolate Reductase (DHFR) were extracted using the Ensembl ID ENSG00000228716. The expression level of DHFR gene in each leukemia cell line was compared to the expression level of the gene in normal cells using log fold change and two-sided Welch's *t*-test.

Docking procedure

Starting conformations of the compounds were built from their SMILES representations using the chemical toolbox Open Babel 2.4.1 (O'Boyle et al., 2011). AutoDock Tools version 1.5.6 was used for docking the target protein DHFR (PDB ID: 2W3M) and compounds (Morris et al., 2009). The torsions of the compounds were defined using the AutoTors utility of AutoDock Tools. Except for amide and ring torsions, all torsions were treated as flexible. Both the protein and the compounds were assigned Gasteiger atomic charges (Gasteiger & Marsili, 1978). Then the non-polar hydrogen atoms were merged.

It was used with AutoDock 4.2 program for comprehensive docking calculations (Morris et al., 2009). AutoGrid program was used to create grid maps with 0.375 Å spacing. The grid center was chosen to coincide with the center of the channel identified with the program PROPORES (Lee & Helms, 2012) The grid dimensions (60 Å × 60 Å × 70 Å) were calculated based on the probe spheres located by PROPORES to represent the channel space (see Figure 2a).

For the docking calculations, standard Lamarckian genetic algorithm protocol was applied with default settings, except for the initial population size, the number of energy evaluations and the number of independent runs, which were increased to obtain more reliable results. Here, our aim was to obtain a single low-energy highly populated cluster to ensure the convergence of the docked results. For the reported results 100 independent calculations were made with an initial population size of 300 randomly placed individuals

and a maximum number of 20 million energy evaluations except for compounds **3bb** and **3e**. For compounds **3bb** and **3e**, we gradually increased the maximum number of energy evaluations to 40 million. In all docking calculations, the starting point of the ligand was randomly created.

Molecular dynamics simulations

The parameters and topologies for the small molecules were derived with the help of Antechamber (Wang et al., 2001, 2006). Python Parser Interface (ACPYPE) (Sousa da Silva & Vranken, 2012). The coordinates for each small molecule were taken from the highest-ranking conformation of the largest cluster. The geometry was optimized using semi-empirical Hamiltonian AM (Pettersen et al., 2004). Afterward, the AM1-BCC charges were derived from the optimized structure (Jakalian et al., 2000; Walker et al., 2008). Equilibrium values and force constants for the bond lengths, angles and dihedrals for the small-molecules were adopted from General Amber Force Field (GAFF) (Wang et al., 2004).

We conducted 100 ns-long conventional molecular dynamics simulations of 10 protein-ligand complexes in explicit solvent using Gromacs package (Van Der Spoel et al., 2005) version 202 (Pronk et al., 2013). We used the top-ranked conformations of the largest clusters that we obtained from molecular docking calculations as starting structures for molecular dynamics simulations. We placed the complex in a cubic box of TIP3P water Jorgensen, 1981) and neutralized the system with the help of counterions when needed. Interactions of protein residues and ions were modeled with the Amber force field F14SB (Maier, 2015). For the short-range non-bonded interactions, we used a cutoff value of 1.2 nm. For long-range electrostatic interactions the particle mesh Ewald (PME) (Essmann et al., 1995) method was utilized. Dispersion correction was applied to both energy and pressure. Periodic boundary conditions were applied in all directions.

For energy minimisation we performed 1000 steps of conjugate gradient algorithm where in every 10 steps one step of steepest descent was carried out. After minimisation, we equilibrated each system using 100 ps of molecular dynamics simulations in NVT ensemble where we restrained the heavy atoms of the protein harmonically using a force constant of 1000 kJ mol^{-1} nm^{-2}. The temperature was maintained at 300 K using velocity rescaling algorithm (Bussi et al., 2007) with a coupling time of 0.5 ps. Solute and solvent atoms were coupled separately to temperature baths. All bonds were constrained using the LINCS algorithm (Hess, 2008). A leap-frog algorithm with a time step of 2 fs was used for integrating Newton's equations of motion. For data collection NPT ensemble was employed in the absence of any restraints. The pressure was kept at 1 bar using Parrinello-Rahman barostat (Parrinello & Rahman, 1981) with a time constant of 0.5 ps. The temperature was regulated using Nose-Hoover temperature coupling method (Hoover, 1985; Nose, 1984) where the reference temperature and the time constant were set to 300 and 0.5 ps, respectively.

The resulting trajectories were utilized for further analyses where the first 3 ns was assumed to be relaxation phase and omitted.

Ligand conformation of the first frame in the trajectory was taken as reference structure for RMSD calculations after aligning only the protein conformations. Values given in parenthesis stand for standard deviations.

Binding free energy calculations

The MM(PB/GB)SA approach is an end-point method that combines gas phase energy contributions, solvation free energy components calculated from an implicit solvent model for complex, receptor and ligand (Kollman et al., 2000). Solute entropy contributions to the total free energy are added as a further refinement.

In this study, we followed the single trajectory approach to compute binding free energies for the molecules. The first 3 ns of each trajectory was taken as equilibrium and therefore omitted. Explicit solvent and ions were stripped from trajectory files before the free energy calculations. The complex topology files were generated using tleap module of AmberTools, version 22 (Case et al., 2018). Topology file for each species was generated with the script ante-MMPBSA.py. The calculations were performed using MMPBSA.py script (Miller et al., 2012) of AmberTools22. The gas phase free energy contributions were calculated using Sander program within AmberTools22.

In order to compute the polar contribution of solvation free energy, we used GB-OBC continuum solvent model developed by Onufriev et al. (2000) where the parameters α, β, γ were set to 1.0, 0.8, and 4.85, respectively (Onufriev et al., 2004). For effective Born radii we used mbondi2 radii as suggested by Onufriev et al. (Weiser et al., 1999). The nonpolar contribution to solvation free energy was approximated by the LCPO method (Laskowski & Swindells, 2011). Translational, rotational, and vibrational entropies were computed separately and added together to approximate the configurational entropy for the solute.

Translational and rotational entropies were calculated from their gas phase partition functions. Frequencies of vibrational modes were obtained using normal-mode analysis after energy minimisation of the snapshots. Entropy contributions were averaged over 100 snapshots.

The standard errors for the MMGBSA effective energy and the solute entropy were combined in quadrature to obtain standard error for the binding free energy. Then, the computed standard error was used to construct 95% Welch–Satterthwaite confidence interval for the free energy of binding.

ACKNOWLEDGMENTS

We would like to thank the late Prof.Dr. Nuket Ocal for this project.

FUNDING INFORMATION

Generous financial support from the TÜBİTAK (project no: 117Z307) is gratefully acknowledged.

CONFLICT OF INTEREST STATEMENT

This manuscript has no known competing financial interests or personal relationships that could have appeared to influence the work reported.

DATA AVAILABILITY STATEMENT

The data that supports the findings of this study are available in the supplementary material of this article

ORCID

Oznur Eyilcim https://orcid.org/0000-0001-6222-960X
Fulya Gunay https://orcid.org/0000-0002-8539-949X
Omer Tahir Gunkara https://orcid.org/0000-0003-3528-5045
Yuk Yin Ng https://orcid.org/0000-0001-9755-6045
Ozlem Ulucan https://orcid.org/0000-0002-7442-5728
Ihsan Erden https://orcid.org/0000-0001-6267-6346

REFERENCES

Acharya, A., Anumandla, D., & Jeffrey, C. S. (2015). Dearomative indole cycloaddition reactions of aza-oxyallyl cationic intermediates: Modular access to pyrroloindolines. *Journal of the American Chemical Society*, *137*(47), 14858–14860. https://doi.org/10.1021/jacs.5b10184

Acharya, A., Eickhoff, J. A., Chen, K., Catalano, V. J., & Jeffrey, C. S. (2016). Access to bicyclic hydroxamate macrocycles via intramolecular aza-(4 + 3) cyloaddition reactions of aza-oxyallylic cation intermediates. *Organic Chemistry Frontiers*, *3*, 330–334. https://doi.org/10.1039/C5QO00315F

Acharya, A., Eickhoff, J. A., & Jeffrey, C. S. (2013). Intramolecular aza-[4 + 3] cycloaddition reactions of α-halohydroxamates. *Synthesis*, *45*(13), 1825–1836. https://doi.org/10.1055/s-0033-1338883

Acharya, A., Montes, K., & Jeffrey, C. S. (2016). Access to 4-oxazolidinones: A (3 + 2) cycloaddition approach. *Organic Letters*, *18*, 6082–6085. https://doi.org/10.1021/acs.orglett.6b03069

Almerico, A. M., Mingoia, F., Diana, P., Barraja, P., Lauria, A., Montalbano, A., Cirrincione, G., & Dattolo, G. (2005). 1-methyl-3*H*-pyrazolo[1,2-a]benzo[1,2,3,4]tetrazin-3-ones. Design, synthesis, and biological activity of new antitumor agents. *Journal of Medicinal Chemistry*, *48*, 2859–2866. https://doi.org/10.1021/jm049075u

An, Y., Xia, H., & Wu, J. (2016). Base-controlled [3 + 3] cycloaddition of isoquinoline *N*-oxides with azaoxyallyl cations. *Chemical Communications*, *52*, 10415–10418. https://doi.org/10.1039/C6CC03650C

Banerjee, D., Mayer-Kuckuk, P., Capiaux, G., Budak-Alpdogan, T., Gorlick, R., & Bertino, J. R. (2002). Novel aspects of resistance to drugs targeted to dihydrofolate reductase and thymidylate synthase. *Biochimica et Biophysica Acta*, *1587*(2–3), 164–173. https://doi.org/10.1016/s0925-4439(02)00079-0

Barnes, K. L., Koster, A. K., & Jeffrey, C. S. (2014). Trapping the elusive aza-oxyallylic cation: New opportunities in heterocycloaddition chemistry. *Tetrahedron Letters*, *55*, 4690–4696. https://doi.org/10.1016/j.tetlet.2014.06.050

Bussi, G., Donadio, D., & Parrinello, M. (2007). Canonical sampling through velocity rescaling. *The Journal of Chemical Physics*, *126*(1), 014101. https://doi.org/10.1063/1.2408420

Carvalho, B. S., & Irizarry, R. A. (2010). A framework for oligonucleotide microarray preprocessing. *Bioinformatics*, *26*(19), 2363–2367. https://doi.org/10.1093/bioinformatics/btq431

Case, D. A., Ben-Shalom, I. Y., Brozell, S. R., Cerutti, D. S., Cheatham, T. E., III, Cruzeiro, V. W. D., Darden, T. A., Duke, R. E., Ghoreishi, D., Gilson, M. K., Gohlke, H., Goetz, A. W., Greene, D., Harris, R., Homeyer, N., Izadi, S., Kovalenko, A., Kurtzman, T., Lee, T. S., … Kollman, P. A. (2018). *Amber 18*. University of California.

Cheng, X., Cao, X., Xuan, J., & Xiao, W. J. (2018). Silver(I)- and base-mediated [3 + 3]-cycloaddition of C,N-cyclic azomethine imines with aza-oxyallyl cations. *Organic Letters*, *20*(1), 52–55. https://doi.org/10.1021/acs.orglett.7b03344

Cory, A. H., Owen, T. C., Barltrop, J. A., & Cory, J. G. (1991). Use of an aqueous soluble tetrazolium/formazan assay for cell growth assays in culture. *Cancer Communications*, *3*(7), 207–212. https://doi.org/10.3727/095535491820873191

Dai, Z. C., Chen, Y. F., Zhang, M., Li, S. K., Yang, T. T., Shen, L., Wang, J. X., Qian, S. S., Zhu, H. L., & Ye, Y. H. (2015). Synthesis and antifungal activity of 1,2,3-triazole phenylhydrazone derivatives. *Organic & Biomolecular Chemistry*, *13*, 477–486. https://doi.org/10.1039/C4OB01758G

DiPoto, M. C., Hughes, R. P., & Wu, J. (2015). Dearomative indole (3 + 2) reactions with azaoxyallyl cations—New method for the synthesis of pyrroloindolines. *Journal of the American Chemical Society*, *137*(47), 14861–14864. https://doi.org/10.1021/jacs.5b10221

DiPoto, M. C., & Wu, J. (2018). Synthesis of 2-aminoimidazolones and Imidazolones by (3 + 2) annulation of azaoxyallyl cations. *Organic Letters*, *20*(3), 499–501. https://doi.org/10.1021/acs.orglett.7b03719

Dulucq, S., St-Onge, G., Gagné, V., Ansari, M., Sinnett, D., Labuda, D., Moghrabi, A., & Krajinovic, M. (2008). DNA variants in the dihydrofolate reductase gene and outcome in childhood ALL. *Blood*, *111*(7), 3692–3700. https://doi.org/10.1182/blood-2007-09-110593

Essmann, U., Perera, L., & Berkowitz, M. L. (1995). A smooth particle mesh Ewald method. *The Journal of Chemical Physics*, *103*(19), 8577–8593. https://doi.org/10.1063/1.470117

Gasteiger, J., & Marsili, M. (1978). A new model for calculating atomic charges in molecules. *Tetrahedron Letters*, *19*(34), 3181–3184. https://doi.org/10.1016/S0040-4039(01)94977-9

Greenberg, J. M., Gonzalez-Sarmiento, R., Arthur, D. C., Wilkowski, C. W., Streifel, B. J., & Kersey, J. H. (1988). Immunophenotypic and cytogenetic analysis of Molt-3 and Molt-4: Human T-lymphoid cell lines with rearrangement of chromosome 7. *Blood*, *72*(5), 1755–1760. https://doi.org/10.1182/blood.V72.5.1755.bloodjournal7251755

Hess, B. (2008). P-LINCS: A parallel linear constraint solver for molecular simulation. *Journal of Chemical Theory and Computation*, *4*(1), 116–122. https://doi.org/10.1021/ct700200b

Hoover, W. G. (1985). Canonical dynamics – Equilibrium phase-space distributions. *Physical Review A*, *31*(3), 1695–1697. https://doi.org/10.1103/PhysRevA.31.1695

Hu, W., Rao, G., & Sun, Y. (2004). Synthesis and antitumor activity of s-tetrazine derivatives. *Bioorganic & Medicinal Chemistry Letters*, *14*(5), 1177–1181. https://doi.org/10.1016/j.bmcl.2003.12.056

Hu, W., Shi, H., Yuan, Q., & Sun, Y. (2005). Synthesis and antitumor activity of *N*,*N*′-bis(substitutedphenyl)-3, 6-dialkyl-1,4-dihydro-s-tetrazine-1,4-dicarboxamide. *Journal of Chemical Research*, *2*, 91–93. https://doi.org/10.1002/chin.200536168

Jakalian, A., Bush, B. L., Jack, D. B., & Bayly, C. I. (2000). Fast, efficient generation of high-quality atomic charges. AM1-BCC model: I. method. *Journal of Computational Chemistry*, *21*(2), 132–146. doi:10.1002/(SICI)1096-987X(20000130)21:2<132::AID-JCC5>3.0.CO;2-P

Jeffrey, C. S., Barnes, K. L., Eickhoff, J. A., & Carson, C. R. (2011). Generation and reactivity of aza-oxyallyl cationic intermediates: Aza-[4 + 3] cycloaddition reactions for heterocycle synthesis. *Journal of the American Chemical Society*, *133*(20), 7688–7691. https://doi.org/10.1021/ja201901d

Ji, W., Liu, Y. A., & Liao, X. (2016). Transition-metal-free synthesis of *N*-hydroxy oxindoles by an aza-Nazarov-type reaction involving azaoxyallyl cations. *Angewandte Chemie International Edition*, *55*(42), 13286–13290. https://doi.org/10.1002/anie.201607177

Ji, W., Yao, L., & Liao, X. (2016). Access to the pyrroloindoline core via [3 + 2] annulation as well as the application in the synthetic approach to (±)-minfiensine. *Organic Letters*, *18*(3), 628–630. https://doi.org/10.1021/acs.orglett.5b03421

Jia, Q., Du, Z., Zhang, K., & Wang, J. (2017). [3 + 2] cycloaddition of aza-oxyallyl cations with aldehydes. *Organic Chemistry Frontiers*, *4*, 91–94. https://doi.org/10.1039/C6QO00526H

Jiang, S., Li, K., Yan, J., Shi, K., Zhao, C., Yang, L., & Zhong, G. (2017). Synthetic access to oxazolidin-4-ones via elimination/[3 + 2] cycloaddition reaction. *The Journal of Organic Chemistry*, *82*(18), 9779–9785. https://doi.org/10.1021/acs.joc.7b00547

Jinjun, S., Kantoff, P. W., Wooster, R., & Farokhzad, O. C. (2017). Cancer nanomedicine: Progress, challenges and opportunities. *Nature Reviews Cancer*, *17*, 20–37. https://doi.org/10.1038/nrc.2016.108

Jorgensen, W. (1981). Transferable intermolecular potential functions for water, alcohols, and ethers. Application to liquid water. *Journal of the American Chemical Society*, *103*(2), 335–340. https://doi.org/10.1021/ja00392a016

Keiser, M. J., Roth, B. L., Armbruster, B. N., Ernsberger, P., Irwin, J. J., & Shoichet, B. K. (2007). Relating protein pharmacology by ligand chemistry. *Nature Biotechnology*, *25*(2), 197–206. https://doi.org/10.1038/nbt1284

Kollman, P. A., Massova, I., Reyes, C., Kuhn, B., Huo, S., Chong, L., Lee, M., Lee, T., Duan, Y., Wang, W., Donini, O., Cieplak, P., Srinivasan, J., Case, D. A., & Cheatham, T. E. (2000). Calculating structures and free energies of complex molecules: Combining molecular mechanics and continuum models. *Accounts of Chemical Research*, *33*(12), 889–897. https://doi.org/10.1021/ar000033j

Laskowski, R. A., & Swindells, M. B. (2011). LigPlot+: Multiple ligand-protein interaction diagrams for drug discovery. *Journal of Chemical Information and Modeling*, *51*(10), 2778–2786. https://doi.org/10.1021/ci200227u

Lee, P. H., & Helms, V. (2012). Identifying continuous pores in protein structures with PROPORES by computational repositioning of gating residues. *Proteins*, *80*(2), 421–432. https://doi.org/10.1002/prot.23204

Li, C., Jiang, K., Ouyang, Q., Liu, T., & Chen, Y. C. (2016). [3 + 1]- and [3 + 2]-cycloadditions of azaoxyallyl cations and sulfur ylides. *Organic Letters*, *18*(11), 2738–2741. https://doi.org/10.1021/acs.orglett.6b01194

Lowery, C. A., Park, J., Kaufmann, G. F., & Janda, K. D. (2008). An unexpected switch in the modulation of AI-2-based quorum sensing discovered through synthetic 4,5-dihydroxy-2,3-pentanedione analogues. *Journal of the American Chemical Society*, *130*(29), 9200–9201. https://doi.org/10.1021/ja802353j

Maier, J. A., Martinez, C., Kasavajhala, K., Wickstrom, L., Hauser, K. E., & Simmerling, C. (2015). ff14SB: Improving the accuracy of protein side chain and backbone parameters from ff99SB. *Journal of Chemical Theory and Computation*, *11*(8), 3696–3713. https://doi.org/10.1021/acs.jctc.5b00255

Matheson, E. C., Hogarth, L. A., Case, M. C., Irving, J. A., & Hall, A. G. (2007). DHFR and MSH3 co-amplification in childhood acute lymphoblastic leukaemia, in vitro and in vivo. *Carcinogenesis*, *28*(6), 1341–1346. https://doi.org/10.1093/carcin/bgl235

Miller, B. R., McGee, T. D., Swails, J. M., Homeyer, N., Gohlke, H., & Roitberg, A. E. (2012). MMPBSA.Py: An efficient program for end-state free energy calculations. *Journal of Chemical Theory and Computation*, *8*(9), 3314–3321. https://doi.org/10.1021/ct300418h

Morris, G. M., Huey, R., Lindstrom, W., Sanner, M. F., Belew, R. K., Goodsell, D. S., & Olson, A. J. (2009). AutoDock4 and AutoDockTools4: Automated docking with selective receptor flexibility. *Journal of Computational Chemistry*, *30*(16), 2785–2791. https://doi.org/10.1002/jcc.21256

Neunhoeffer, H. (1985). Six-membered rings with oxygen, sulfur or two or more nitrogen atoms. In *Comprehensive heterocyclic chemistry I* (Vol. *3*). Pergamon.

Nhu, D., Duffy, S., Avery, V. M., Hughes, A., & Baell, J. B. (2010). Antimalarial 3-arylamino-6-benzylamino-1,2,4,5-tetrazines. *Bioorganic & Medicinal Chemistry Letters*, *20*, 4496–4498. https://doi.org/10.1016/j.bmcl.2010.06.036

Nose, S. (1984). Unified formulation of the constant temperature molecular-dynamics methods. *The Journal of Chemical Physics*, *81*(1), 511–519. https://doi.org/10.1063/1.447334

O'Boyle, N. M., Banck, M., James, C. A., Morley, C., Vandermeersch, T., & Hutchison, G. R. (2011). Open babel: An open chemical toolbox. *Journal of. Chem*, *3*(33). https://doi.org/10.1186/1758-2946-3-33

Onufriev, A., Bashford, D., & Case, D. A. (2000). Modification of the generalized born model suitable for macromolecules. *The Journal of Physical Chemistry B*, *104*(15), 3712–3720. https://doi.org/10.1021/jp994072s

Onufriev, A., Bashford, D., & Case, D. A. (2004). Exploring protein native states and large-scale conformational changes with a modified generalized born model. *Proteins: Structure, Function, and Genetics*, *55*(2), 383–394. https://doi.org/10.1002/prot.20033

Organista-Nava, J., Gómez-Gómez, Y., Illades-Aguiar, B., Rivera-Ramírez, A. B., Saavedra-Herrera, M. V., & Leyva-Vázquez, M. A. (2018). Overexpression of dihydrofolate reductase is a factor of poor survival in acute lymphoblastic leukemia. *Oncology Letters*, *15*(6), 8405–8411. https://doi.org/10.3892/ol.2018.8429

Parrinello, M., & Rahman, A. (1981). Polymorphic transitions in single-crystals - a new molecular-dynamics method. *Journal of Applied Physics*, *52*(12), 7182–7190. https://doi.org/10.1063/1.328693

Pettersen, E. F., Goddard, T. D., Huang, C. C., Couch, G. S., Greenblatt, D. M., Meng, E. C., & Ferrin, T. E. (2004). UCSF chimera–a visualization system for exploratory research and analysis. *Journal of Computational Chemistry*, *25*(13), 1605–1612. https://doi.org/10.1002/jcc.20084

Pronk, S., Páll, S., Schulz, R., Larsson, P., Bjelkmar, P., Apostolov, R., Shirts, M. R., Smith, J. C., Kasson, P. M., van der Spoel, D., Hess, B., & Lindahl, E. (2013). GROMACS 4.5: A high-throughput and highly parallel open source molecular simulation toolkit. *Bioinformatics*, *29*(7), 845–854. https://doi.org/10.1093/bioinformatics/btt055

Ram, V. J., Sethi, A., Nath, M., & Pratap, R. (2019). *The chemistry of heterocycles: Chemistry of six to eight membered N, O, S, P and Se heterocycles* (1st ed.). Elsevier.

Rao, G. W., Wang, C., Wang, J., Zhao, Z. G., & Hu, W. X. (2013). Synthesis, structure analysis, antitumor evaluation and 3D-QSAR studies of 3,6-disubstituted-dihydro-1,2,4,5-tetrazine derivatives. *Bioorganic & Medicinal Chemistry Letters*, *23*, 6474–6480. https://doi.org/10.1016/j.bmcl.2013.09.036

Shao, P. L., Li, Z. R., Wang, Z. P., Zhou, M. H., Wu, Q., Hu, P., & He, Y. (2017). [3 + 2] cycloaddition of azaoxyallyl cations with cyclic ketones: Access to spiro-4-oxazolidinones. *The Journal of Organic Chemistry*, *82*(19), 10680–10686. https://doi.org/10.1021/acs.joc.7b01728

Siegel, R. L., Miller, K. D., & Jemal, A. (2015). Cancer statistics. *CA: A Cancer Journal for Clinicians*, *65*, 5–29. https://doi.org/10.3322/caac.21254

Sauer, J. (1996). 1,2,4,5-Tetrazines. In *Comprehensive heterocyclic chemistry II* (Vol. *6*). Elsevier.

Sousa da Silva, A. W., & Vranken, W. F. (2012). ACPYPE – AnteChamber PYthon parser interfacE. *BMC Research Notes*, *5*, 367. https://doi.org/10.1186/1756-0500-5-367

Swetha, M., Venkata Ramana, P., & Shirodkar, S. G. (2011). Simple and efficient method for the synthesis of azides in water-THF solvent system. *Organic Preparations and Procedures International*, *43*(4), 348–353. https://doi.org/10.1080/00304948.2011.594002

Tabassum, S., Parveen, M., Ali, A., Alam, M., Ahmad, A., Khan, A. U., & Khan, R. A. (2012). Synthesis of aryl-1,2,4,5-tetrazinane-3-thiones, in vitro DNA binding studies, nuclease activity and its antimicrobial activity. *Journal of Molecular Structure*, *1020*, 33–40. https://doi.org/10.1016/j.molstruc.2012.03.049

Van Der Spoel, D., Lindahl, E., Hess, B., Groenhof, G., Mark, A. E., & Berendsen, H. J. C. (2005). GROMACS: Fast, flexible, and free. *Journal of Computational Chemistry*, *26*(16), 1701–1718. https://doi.org/10.1002/jcc.20291

Vanneman, M., & Dranoff, G. (2012). Combining immunotherapy and targeted therapies in cancer treatment. *Nature Reviews Cancer*, *12*, 237–251. https://doi.org/10.1038/nrc3237

Walker, R. C., Crowley, M. F., & Case, D. A. (2008). The implementation of a fast and accurate QM/MM potential method in Amber. *Journal of Computational Chemistry*, *29*(7), 1019–1031. https://doi.org/10.1002/jcc.20857

Wan, Y., Li, Y., Yan, C., Yan, M., & Tang, Z. (2019). Indole: A privileged scaffold for the design of anti-cancer agents. *European Journal of Medicinal Chemistry*, *183*, 111691. https://doi.org/10.1016/j.ejmech.2019.111691

Wang, J., Wolf, R. M., Caldwell, J. W., Kollman, P. A., & Case, D. A. (2004). Development and testing of a general amber force field. *Journal of Computational Chemistry*, *25*(9), 1157–1174. https://doi.org/10.1002/jcc.20035

Wang, J. M., Wang, W., Kollman, P. A., & Case, D. A. (2001). Antechamber: An accessory software package for molecular mechanical calculations. *Journal of the American Chemical Society*, *222*, 403.

Wang, J. W., Kollman, P. A., & Case, D. A. (2006). Automatic atom type and bond type perception in molecular mechanical calculations. *Journal of Molecular Graphics & Modelling*, *25*(2), 247–260. https://doi.org/10.1016/j.jmgm.2005.12.005

Weiser, J., Shenkin, P. S., & Still, W. C. (1999). Approximate atomic surfaces from linear combinations of pairwise overlaps (LCPO). *Journal of Computational Chemistry*, *20*(2), 217–230. https://doi.org/10.1002/(SICI)1096-987X(19990130)20:2<217::AID-JCC4>3.0.CO;2-A

Wishart, D. S., Knox, C., Guo, A. C., Shrivastava, S., Hassanali, M., Stothard, P., Chang, Z., & Woolsey, J. (2006). DrugBank: A comprehensive resource for in silico drug discovery and exploration. *Nucleic Acids Research*, *34*, 668–672. https://doi.org/10.1093/nar/gkj067

Xu, X., Zhang, K., Li, P., Yao, H., & Lin, A. (2018). [3 + 3] cycloaddition of azides with in situ formed azaoxyallyl cations to synthesize 1,2,3,4-tetrazines. *Organic Letters*, *20*(7), 1781–1784. https://doi.org/10.1021/acs.orglett.8b00280

Zlotin, S. G., Churakov, A. M., Luk'yanov, O. A., Makhova, N. N., Yu Sukhorukov, A., & Tartakovsky, V. A. (2015). Novel approaches to pharmacology-oriented and energy rich organic nitrogen–oxygen systems. *Mendeleev Communication*, *25*, 399–409. https://doi.org/10.1016/j.mencom.2015.11.001

SUPPORTING INFORMATION

Additional supporting information can be found online in the Supporting Information section at the end of this article.

How to cite this article: Eyilcim, O., Gunay, F., Gunkara, O. T., Ng, Y. Y., Ulucan, O., & Erden, I. (2023). Design and synthesis of novel 1,2,3,4-tetrazines as new anti-leukemia cancer agents. *Chemical Biology & Drug Design*, *102*, 1186–1201. https://doi.org/10.1111/cbdd.14328